Geoscience Frontiers 10 (2019) 957–971

HOSTED BY

Contents lists available at ScienceDirect

China University of Geosciences (Beijing)

Geoscience Frontiers

journal homepage: www.elsevier.com/locate/gsf

Research Paper

High resolution facies architecture and digital outcrop modeling of the Sandakan formation sandstone reservoir, Borneo: Implications for reservoir characterization and flow simulation

Numair A. Siddiqui [a,*], Mu. Ramkumar [b], Abdul Hadi A. Rahman [a], Manoj J. Mathew [c], M. Santosh [d,e], Chow W. Sum [a], David Menier [f]

[a] Department of Petroleum Geosciences, Universiti Teknologi PETRONAS, Bandar Seri Iskandar, 31750 Tronoh, Perak, Malaysia
[b] Department of Geology, Periyar University, Salem 636011, India
[c] Institute of Oceanography and Environment, Universiti Malaysia Terengganu, 21030, Kuala Nerus, Terengganu, Malaysia
[d] Department of Earth Sciences, University of Adelaide, SA 5005, Australia
[e] School of Earth Sciences and Resources, China University of Geosciences Beijing, 29 Xueyuan Road, Beijing 100083, China
[f] Laboratoire Géosciences Océan, UMR CNRS 6538, Campus de Tohannic, 56000 Vannes, France

ARTICLE INFO

Article history:
Received 3 November 2017
Received in revised form
12 February 2018
Accepted 14 April 2018
Available online 26 May 2018
Handling Editor: E. Shaji

Keywords:
Siliciclastic sandstone facies
Connectivity
Heterogeneity
Digital outcrop model
Flow dynamics

ABSTRACT

Advances in photogrammetry have eased the acquisition of high-resolution digital information from outcrops, enabling faster, non-destructive data capturing and improved reservoir modeling. Geocellular models for flow dynamics with in the virtual outcrop in siliciclastic deposits at different sets of sandstone facies architecture remain, however, a challenge. Digital maps of bedding, lithological contrast, spatial-temporal variations of bedding and permeability characteristics make it more easy to understand flow tortuosity in a particular architecture. An ability to precisely model these properties can improve reservoir characterization and flow modeling at different scales. Here we demonstrate the construction of realistic 2D sandstone facies based models for a pragmatic simulation of flow dynamics using a combination of digital point clouds dataset acquired from LiDAR and field investigation of the Sandakan Formation, Sabah, Borneo. Additionally, we present methods for enhancing the accuracy of outcrop digital datasets for producing high resolution flow simulation. A well-exposed outcrop from the Sandakan Formation, Sabah, northwest Borneo having a lateral extent of 750 m was chosen in order to implement our research approach. Sandstone facies and its connectivity are well constrained by outcrop observations, data from air-permeability measurements, bilinear interpolation of permeability, grid construction and water vector analysis for flow dynamics. These proportions were then enumerated in terms of static digital outcrop model (DOM) and facies model based on sandstone facies bedding characteristics. Flow simulation of water vector analysis through each of the four sandstone facies types show persistent spatial correlation of permeability that align with either cross-bedded orientation or straight with more dispersion high quality sandstone (porosity 21.25%–41.2% and permeability 1265.20–5986.25 mD) and moderate quality sandstone (porosity 10.44%–28.75% and permeability 21.44–1023.33 mD). Whereas, in more heterolithic sandstone (wavy- to flaser-bedded and bioturbated sandstone), lateral variations in permeability show spatially non-correlated patterns over centimeters to tens of meters with mostly of low quality sandstone (porosity 3.4%–12.31% and permeability < 1 mD to 3.21 mD). These variations reflect the lateral juxtaposition in flow dynamics. It has also been resulted that the vertical connectivity and heterogeneities in terms of flow are mostly pragmatic due to the interconnected sandstone rather than the quality of sandstone.

1. Introduction

Reservoir modeling is a priori requirement for hydrocarbon exploration, production and enhanced recovery (Clemetsen et al., 1990; Alexander, 1993; Egeland et al., 1993; MacDonald and

* Corresponding author.
E-mail addresses: numairpng@gmail.com, numairsidd717@gmail.com (N.A. Siddiqui).
Peer-review under responsibility of China University of Geosciences (Beijing).

https://doi.org/10.1016/j.gsf.2018.04.008

Halland, 1993; Liu et al., 1996; Caers et al., 2000; Caers and Zhang, 2004; Miall, 2006; Fabuel-Perez et al., 2010). Conventional datasets such as seismic and well data used in reservoir modeling provide a deterministic architectural framework with facies and petrographic description at discrete locations (Higgs et al., 2010; Hodgetts, 2013; Siddiqui et al., 2015). However, uncertainties exist with heterogeneities related to the sandstone facies distribution (Krum and Johnson, 1993; Hurst et al., 1999; Slatt and Weimer, 1999; Slatt et al., 2000; Falivene et al., 2006; Siddiqui et al., 2014, 2016; Newell and Shariatipour, 2016; Siddiqui et al., 2017a,b), which significantly hamper the exploration and production strategies. In order to mitigate these, to understand the architecture style and relationships between facies, and to analyze the internal distribution of permeable and non-permeable sand bodies, outcrop analogues are used (Aigner et al., 1996; Wilson et al., 2011).

Siliciclastic sedimentary rocks from complex architectures of bedding and textural geometries which affect fluid flow by spatial variations in porosity and the arrangements of permeable pathways and barriers. During past few years, new techniques and approaches involving deterministic geological models based on outcrop analogues (e.g. Hodgetts, 2013; Sima, 2013) have been industrialized. Advances in digital data collection and processing techniques with cost-effective and more sophisticated methods (e.g. Pringle et al., 2006; Buckley et al., 2008; Siddiqui et al., 2017a) were prime contributors for this development. One of these new techniques is the 2D and 3D Light Detecting and Ranging (LiDAR) technique that enables high-resolution digital data capturing from outcrops with which conventional and improved modeling schemes could be attempted (e.g. Buckley et al., 2013; Natali et al., 2013; Howell et al., 2015). The key advantages are high point density and spatial resolution accuracy of acquired data sets, as well as easy applicability for sedimentological and exploration research.

Though several publications describe the collection and processing of LiDAR data (Pringle et al., 2004, 2006; Bellian et al., 2005; Enge et al., 2007; Buckley et al., 2008, 2013; Kurz et al., 2011; Sima, 2013; Howell et al., 2015), few researchers describe the approaches and different uses of digital outcrop models (DOMs) in geological modeling inclusive of flow simulation (Willis and White, 2000; Wilson et al., 2011; Buckley et al., 2013). An array of data sets including conventional field data and novel digital data drawn from hyperspectral imagery and ground penetrating radar were utilized by Hodgetts (2013) for geomodeling. Enge et al. (2007) provided the workflow for modeling deltaic clinoforms. Falivene et al. (2006) demonstrated the stochastic facies modeling techniques for channel-fill turbidite sandstone. Labourdette and Jones (2007) made a first attempt to build facies model of a fluvial braided system by combining Digital Outcrop Model (DOM) with aerial photographs to establish quantitative data on the morphology of geobodies. Results of these studies suggested that simulation studies of high resolution at initial stage of flow modeling need to be identified from different types of sandstones so that effect of fluid flow within a specific architecture, permeability and bedding characteristics can be accurately defined and predicted. Several commercial quantities of hydrocarbon discoveries, mainly in thin-bedded sandstones of Middle and Early Miocene age have been made in the overlapping areas of the Central Sabah and the Sandakan Sub-Basin (Northeast Sabah Basin) (PETRONAS, 1999; Mazlan and Rahman, 2007), making this formation ideal for testing the objectives of the present study. In the Central Sabah Sub-basin, reservoir includes, in addition to the Tanjong, the Sandakan Formation or their equivalents. However, it should be noted that the reservoir quality and architecture vary from very tight to friable, especially where the reservoirs are in lateral continuity with the possible mature source rock (Comexco Inc., 1993). In the Sandakan Sub-basin, the Sandakan Formation exhibits strong depositional facies control on their poro-perm properties. The sandstone had recorded the highest poro-perm (porosity $>$ 20%; permeability $>$ 10 mD), but with very limited lateral and vertical continuity (Majid et al., 2017).

The aim of this paper is to test and produce an accurate description of workflow (from data collection to building flow dynamic model) to present a high resolution models in siliciclastic sandstone facies type with digital point clouds dataset from LiDAR (light detection and ranging) for evaluation of uncertainties and heterogeneities. With these, we try to illustrate the effect of different types of sandstone bedding on fluid dynamics.

2. Geological setting

The offshore Sabah Basin, underlies the continental margin off western Sabah. It is located at northwest Borneo and formed during Middle Miocene. The tectonic evolution of the Sabah Basin was discussed by many workers (Whittle and Short, 1978; Hamilton, 1979; Levell, 1987; Hutchison, 1989, 2005; Tan and Lamy, 1990; Tongkul, 1991, 1992; 1994; Hall, 1996, 2002, 2013; PETRONAS, 1999; Hall and Morley, 2004; Sapin et al., 2011; Franke et al., 2014; Mathew et al., 2016). Towards east Sabah, two significant rifting events, namely, NE trending Sandakan Rift and the SE trending Tarakan Rift contributed towards the development of Sandakan and Tarakan Basin formations (Hall and Morley, 2004; Futalan et al., 2012). The NE Sabah Basin is divided into two deep sedimentation areas which comprise; (i) the central Sabah Sub-basin occupying the 'Sandakan Rift' and consisting of Miocene–Pliocene age sediments, overlies the Labang and/or older formations (Tjia et al., 1990) (Fig. 1a), and (ii) the Sandakan Sub-basin (Bell and Jessop, 1974).

Later, the Sandakan Basin was subjected to NW rifting volcanism and accumulation of chaotic deposits (Futalan et al., 2012). In the east, during Early–Middle Miocene, the Sulu Sea opened, widening the Sandakan Basin as an extensional basin which served as a new and large depocenter (Tongkul, 1991, 1992). This rifting in Sulu Sea ceased during Late-Miocene and caused the uplift of Sandakan Peninsula (Graves and Swauger, 1997; Futalan et al., 2012), heavy erosion and Shallow Regional Unconformity (SRU). Followed up episode of compression closed the newly opened Sulu Sea and resulted in the formation of several NE trending arches that reactivated the deltaic growth fault and created long faulted anticlines.

The sedimentary rocks of the Sandakan Formation cover approximately 70 km^2 (Fig. 1b). It apparently makes up the fill of one of a series of isolated circular "basins" some with diameters of up to 60 km, stretching across eastern Sabah. Paleontological studies indicate that the formation is younger than the Tanjong Formation West (Stauffer, 1967; Lee, 1970) (Fig. 1c). The faunal occurrences are very uncommon, probably due to dissolution, but a few casts of marine bivalves have been found, including *modiolids* and *scallops*. In addition, small crab remains, measuring up to 3 cm in length are commonly occurred. These suggested that the deposition in wave-dominated deltaic setting (Noad and Neil, 1996), shallow marine lagoonal or inter-distributary bay facies, in a relatively sheltered region, protected from open marine conditions. The recent deposits consist of thick layers of carbonaceous clay, silt, sand and pebbles in the present river valleys, deltas and coastal plains (Lee, 1970). The Sandakan Formation comprises more than 2500 m of mudstone, sandstone and siltstone of a Late Miocene or younger age. Sandakan Formation have plenty of primary sedimentary structures (Lee, 1970). According to Chung et al. (2015), the Sandakan

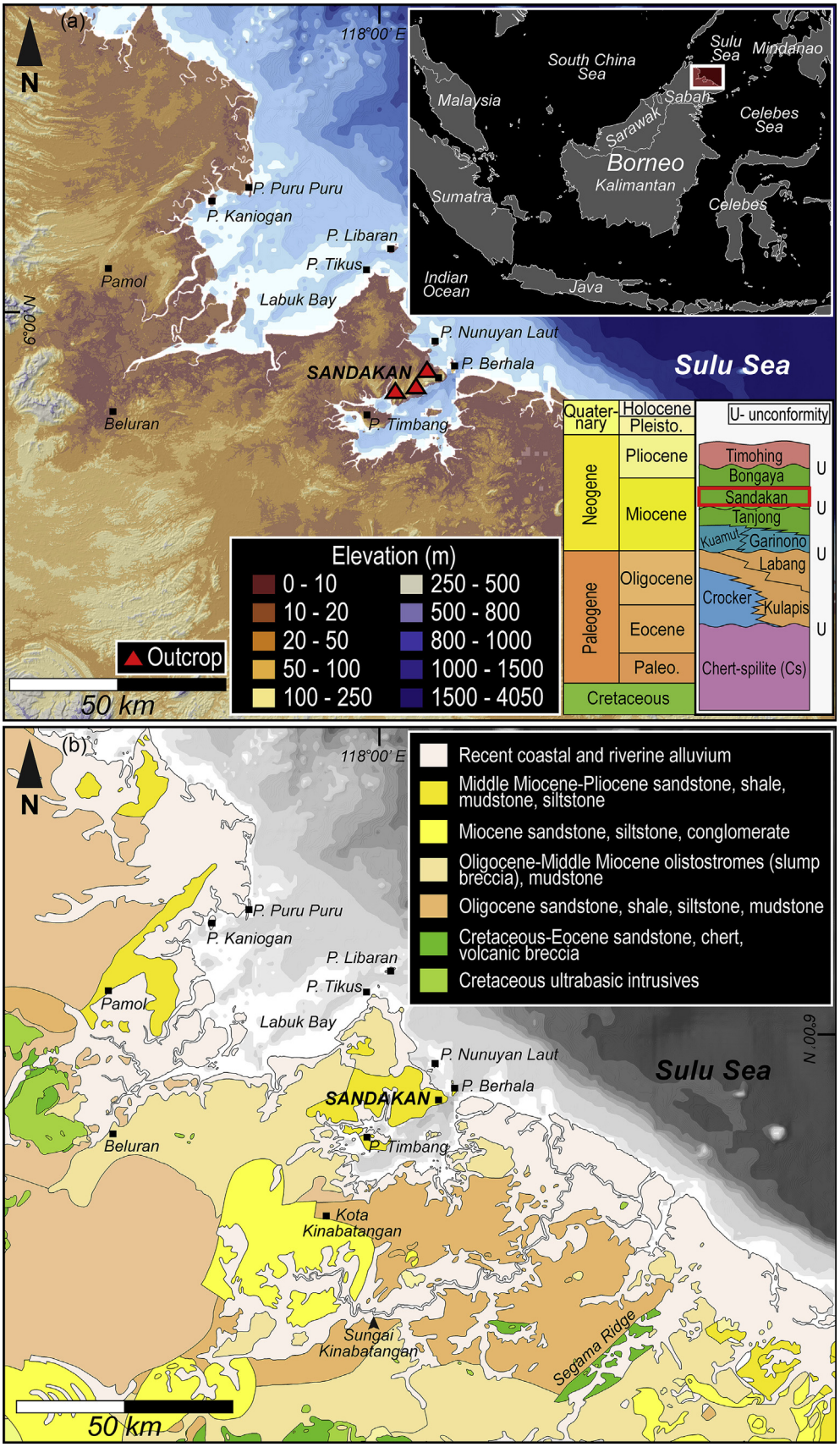

Figure 1. (a) The outcrops location map of the Sandakan Formation (red triangle), Sabah, East Malaysia; with generalized stratigraphic succession from Paleogene–Quatenary sedimentation and Sandakan Formation. The study area occupied near Sandakan with Later Neogene clastic deposits (Tjia et al., 1990); (b) Generalized depositional succession and boundaries from recent coastal deposits to Cretaceous around Sandakan Formation (PETRONAS, 1999).

Formation is represented by shallow marine and shoreface succession. The shoreface sandstone overlies the carbonaceous mudstone. These are thick amalgamated sandstones, thin, lenticular interbeded hummocky cross-stratified sandstones and mudstones laminated mudstone with Rhizophora, trough cross-bedded sandstones laminated mudstones, and mudstones with thin laminated sandstone and siltstone. The structure and fossil content suggest that this formation was deposited mainly in shallow-marine and deltaic environments, probably with a fluvial deposits from the West (Stauffer, 1967; Lee, 1970).

3. Material and methods

3.1. Porosity and permeability measurements

The porosity-permeability analysis was conducted quantitatively using Tiny-perm II for permeability at outcrop face and with the help of mercury Injection Capillary Pressure (MICP) instrument for porosity measurements for rock samples at laboratory. For the measurement of permeability, a portable handheld Tiny-perm II air perm-meter was used to get the data on rock matrix permeability. The permeability was measured at each outcrop with reference to different facies types. About 2000 such measurements were made. The measurements were taken to observe the variation in grain size and change in permeability within different sets of sandstone facies with numbers of grids (discussed in section 3.6). Whereas, the porosity measurement technique is based on the fact that mercury behaves as a non-wetting liquid with solid materials. Mercury penetrates the open pores of a solid sample under the effect of increasing pressure (up to 200 psi). By measuring the quantity of mercury that penetrates the pores of the samples and the equilibrium pressure at which intrusion occurs, the pore volume distribution is calculated as a function of its radius. The relationship between the pore size and the applied pressure, assuming the pore is cylindrical, is expressed as:

$$pr = -2y\cos\theta$$

where r = pore radius;
y = mercury surface tension;
θ = contact angle;
p = absolute applied pressure.

3.2. Creation of DOMs

Conventional field sedimentological and digital data were utilized for this study. The field data include meso-microscale facies distribution, occurrence and association of sedimentary structures and grain sizes characteristics.

The digital dataset used to build the 2D static connectivity model comprises intensity-coded LiDAR point-clouds, global positioning system (GPS) data and digital photographs. These were combined together to construct digital outcrop model (DOM) which was then utilized to attempt sandstone facies flow simulation. The workflow used for the creation of the DOM and sandstone facies flow simulation is depicted in Fig. 2.

3.3. Field data acquisition

Systematic field mapping, followed by selection of suitable spatial-temporally extended exposure for logging, facies interpretation, photographing and LiDAR data acquisition was conducted. The conventional lithology, documentation of sedimentary and tectonic structural information, collection of data on sandstone facies occurrence and associations was also attempted, which in turn was utilized for the interpretation of different environment and facies quality.

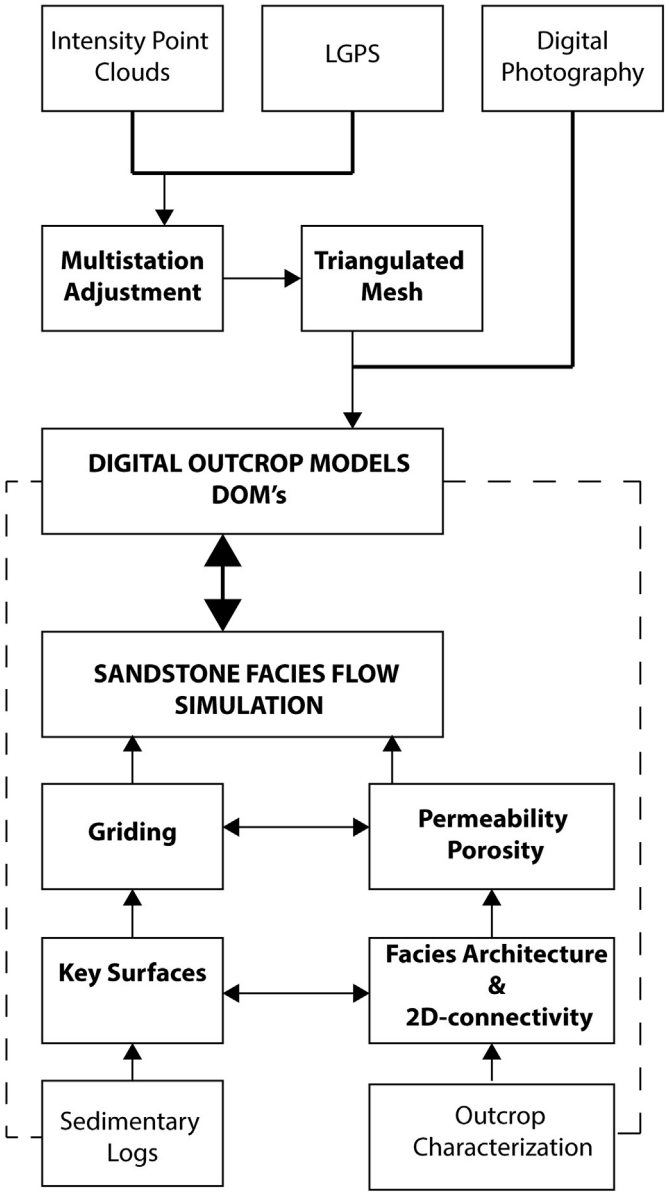

Figure 2. Workflow used in creation of LiDAR DOM (static) and 2D sandstone facies flow simulation model. The input data for DOMs is intensity point clouds and digital photography. Whereas the processing take place by multistation adjustment and triangulated mesh for the construction of draft model. For facies flow simulation, input data of sedimentary logs and outcrop characteristic through field work in conjunction with DOM are used to generate key surfaces and facies architecture with its connectivity.

3.3.1. Instrumentation

RIEGAL 3D laser imaging scanner of LMS-Z series for outcrop scanning and imaging and operated by RiScan pro (v. 1.8.0)® with an accuracy of 0.01 m and a point acquisition rate of up to 10,000 points per second (depending on weather condition and rock reflectivity) was used in this study. A calibrated digital camera (Nikon-100, 12 megapixels), mounted on the laser scanner, allowed acquisition of photographs that were instantly registered and linked to the point-cloud data.

3.3.2. Dataset

The digital dataset acquired in the field includes: (1) intensity-coded LiDAR point-cloud data and (2) digital photographs.

(1) Intensity-coded LiDAR point-cloud data. The LiDAR dataset was collected from a total of 6 scan positions covering an area about 250 m^2 and containing over 10 million points. A GPS system was mounted on the laser scanner, and used for registering the scan positions to the project coordinate system. Each data point records *x*, *y*, *z* position information and intensity attribute values. The intensity depends on the reflectivity of the outcrop face and the distance between the outcrop and the scanner. This was later re-filtered to 0.1 m point spacing to reduce the point-cloud dataset to a manageable size, while retaining more than adequate resolution for the interpretation.
(2) Digital photographs. A total of 50 digital photographs covering the whole study outcrop were acquired during scanning by using digital camera. Images were generated at various magnification scales using 15 mm, 50 mm and 80 mm lenses.

3.4. Consolidation of specific scans

This process allowed the specific scans to be consolidated and accurately located into a single 'global cartesian coordinate system Tie-point method' (TPM). It was carried out by using common points, which were manually picked on adjacent individual scans (Fig. 3a). A minimum of 3–4 points were merged for proper point-cloud merging (Fig. 3b). After all the individual scans were combined and merged, the DGPS information were imported into the project and used to correct and globally position the scan data.

3.5. Tringulating the points

To create a solid surface from point-clouds, the triangulation process was used by connecting the points of different surfaces (Fig. 3c) and to generate the solid horizons of different sandstone facies (Fig. 3d). By mapping each vertex in the mesh back to the digital images, the mesh was textured with those images (Fig. 3e). Each individual pixel within the photographic image were linked its *x*, *y*, *z* coordinate within the correct triangular vertex. In order to avoid large datasets which, become difficult to manipulate interactively and interpret, each fine-scan was divided into small areas that were then textured independently.

3.6. Geocellular grid base flow modeling

Permeability measurements in different sandstone facies at each of the bedding were taken on regular rectangular grids on outcrop sandstone facies wall in dry conditions (Fig. 4a). Mostly all irregularities and weathered or loose material were removed prior to construction of the grids. The measurement spacing was adjusted to the thickness of lamina, so that the vertical and horizontal spacing is between 2 and 5 cm, total grid dimension were between 500 cm and 1 m. An approximately 100–400 air permeability measurements were made (depending the surface exposure, weathering and accessibility of surface) on each sandstone facies and outcrop with different orientation. All permeability data through air-perm II meter and porosity through mercury porosimeter were analyzed and gridded into Petro Mod®2D builder, which in turn were bilinearly interpolated to the entire grid blocks. Bilinear interpolation reflects the nearby 2 × 2 region of known pixel values. Then, a weighted average of these 4 pixels to arrive at its final, interpolated value was attempted. The weightage on each of the 4 pixel values was based on the computed pixel's distance (in 2D space) from each of the known points.

For example, the intensity value at the pixel computed to be at row 15, column 8 can be calculated by linearly interpolating between the values at columns 5 and 10 on each rows 10 and 20 (Fig. 4b), giving:

$$I(10,\ 8) = \frac{(10-8)\times 9.50}{10-5} + \frac{(8-5)\times 10.80}{10-5} = 10.28$$

$$I(20,\ 8) = \frac{(10-8)\times 10.20}{10-5} + \frac{(8-5)\times 11.30}{10-5} = 10.86$$

and then interpolating linearly between these values, giving:

$$I(15,\ 8) = \frac{(20-15)\times 10.28}{20-10} + \frac{(15-10)\times 10.86}{20-10} = 10.57$$

The final output grid base 2D model represents the different quality sandstone and mudstone variations represented in different color codes (Fig. 4c). Finally, the flow models were constructed and analyzed by response-surface methods to synthesize the results, which is simpler and cheaper than fine grid simulations and is more reasonable than using the same pseudofunction for different scenarios (Narayanan et al., 1999).

4. Results

4.1. The Sandakan outcrop: units and sandstone facies

The hierarchy of unit surfaces is recognized in the field and used for correlation between logged section and high resolution LiDAR surfaces (Fig. 5). Four units (1–4), define sandstone facies of the Sandakan Formation in the studied outcrops based on lithology, geometry, sedimentary structures and sandstone quality. A brief description of the facies types is provided herein.

- Hummocky Cross-Stratified Sandstone (HCSS) is characterized by yellowish brown to whitish, very fine- to medium-grained, well sorted sand with an erosive base and a sharp top and bottom, bounded by mudstone (Fig. 5, units 1, 3 and 4). Thickness of this facies varies from 1 to 5 m with continuous clean thick sand, predominately derived from storm-weather wave base deposit. This sandstone displays low angle cross-stratification that can be traced for tens of meters perpendicular to the bedding dip and up to 50 m parallel to bedding dip (Fig. 5).
- Trough cross-bedded sandstone (TCBS) is characterized by yellow to yellowish-gray, very fine- to fine-, moderately-sorted to well-sorted sand. Thickness of this facies varies from 0.5 to 2 m (Fig. 5, unit 1). It forms small scale trough cross-bedding with coal clasts, mixed mud-clasts and mud-drapes. The primary sedimentary structural association suggests deposition in a tide-dominated estuary with a shallow sub-tidal environment.
- The 0.5 m thick, wavy- to flaser-bedded sandstone (W-FBS) is composed of light-yellowish-grey, moderately- to well-sorted, very fine- to silty-sand, and dominated with non-heterolithic bedding. It consists of flaser bedding (typically bifurcated-wavy or, more rarely, wavy) and wavy beddings (Fig. 5, unit 1). The asymmetrical wavy bed forms contain coal laminations within them. These bed-forms are commonly formed in tidal flats where variation of sediment supply and the level of wave (or current) activity occur.
- The 0.5–1 m thick bioturbated sandstone (BS) consists of light-grey to white, fine- to very fine-grained, very well-sorted sand distributed throughout the units with less index of appearance. This facies has a moderate to a very high degree of bioturbation and is also identified with low angle hummocky cross-

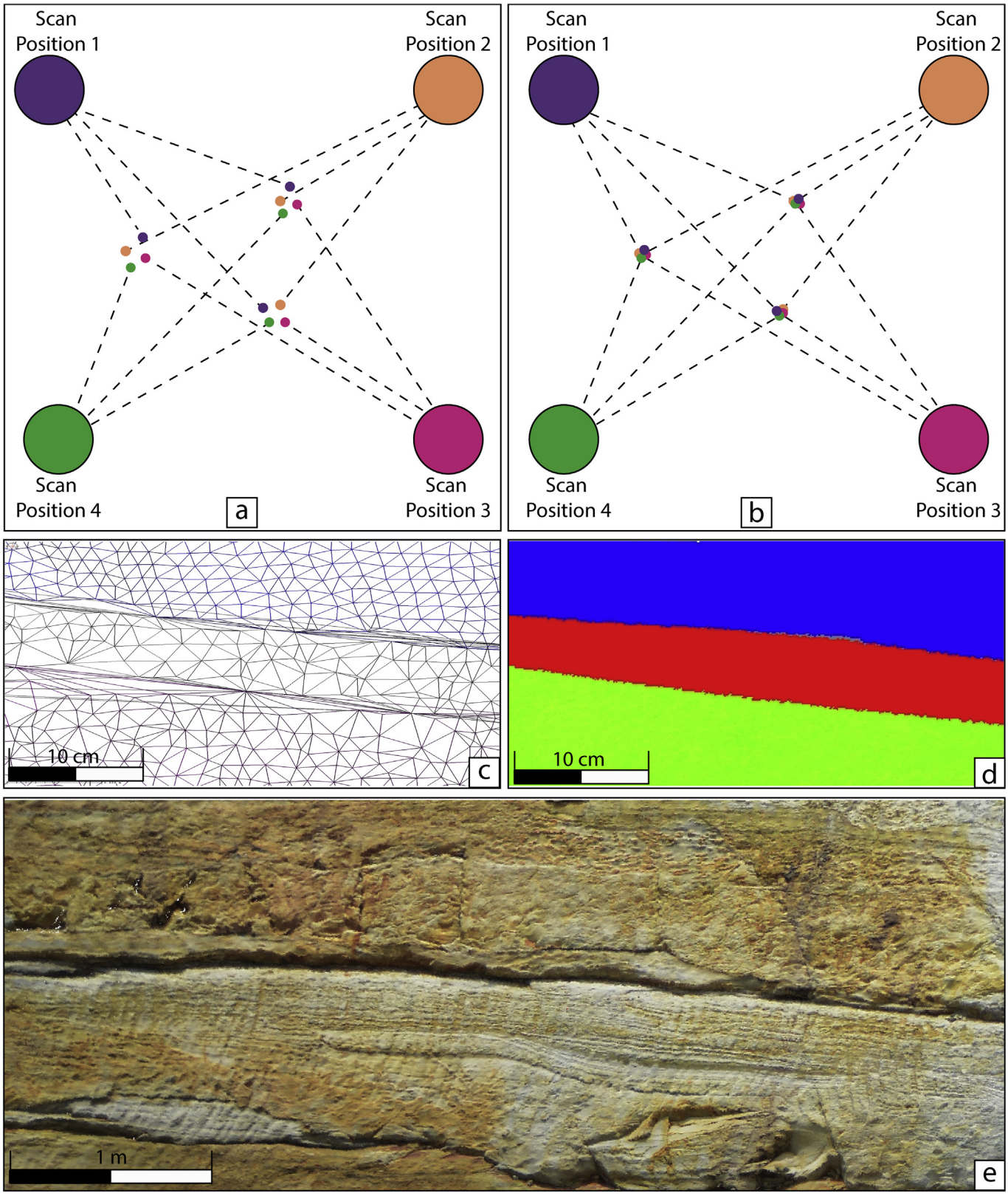

Figure 3. (a) Pre-merging and multi station adjustment of four different scan positions; (b) post-merging and adjustment after data filtration and processing for high resolution outcrop architectural analysis; (c) triangulation of point clouds of a same facies marked with different sets of horizons; (d) connecting and filling in the triangles with different color code to represent the variation in facies distribution; (e) meshing with digital image or photograph for outcrop architecture at high resolution.

stratification. It is characterized by thin layers of fine-grained sandstone.

- Massive Sandstone (MS) facies consists of well-sorted, fine- to very-fine sand with no internal structures. It occurs as individual beds that are separated by mudstone (Fig. 5) in units 1, 2 and 4. The loose, grain-supported framework suggests that the sandstone had modest compaction and shows dewatering structures, suggesting that deposition was in a fluidized condition.

4.2. Outcrop sandstone facies architecture and DOM

The outcrop under study is 112–180 m thick and a lateral extent of about 750 m, with a NW–SE, orientation sub parallel down-dip (038° to 045°). It is divided into four major units with coarsening upward trends (Fig. 6a and b). The outcrop is cut by two normal faults perpendicular to palaeoflow (Fig. 6b and c). The unit one has an average thickness of 36.6 m and is characterized by sandstone facies of HCSS, MS and TCBS with amalgamation of WFBS. The mudstone shows thickness of <1 m (Fig. 5), and sandy facies, which thicken upward, which varies from 10 m thick at base and 4 m at top (Fig. 6b and c).

The units two and three have an average thickness of 47 m separated by two normal faults. They are characterized by mudstone with amalgamation of thin bedded sandstones facies of MS and HCSS and low intensity bioturbation (Fig. 6d). Both units have sharp base and top with coarsening upward intervals. They are traced laterally and vertically by thick mudstone (Figs. 5 and 6d), hummocky cross-stratification and thin coal lamination.

The unit four has an average thickness of 26 m. Its base is represented by the first occurrences of BS and WFBS facies. The next interval is characterized by alternation of two sandstone packages down dipping with 45°, composed of HCSS and TCBS, intercalated with several thin to thick laterally continuous mudstone acting as boundaries between sandstone packages (Fig. 6a and d). The top most package of this unit is 5 m thick MS with coarsening upward trend and no primary internal bedding characteristics followed by thick vegetation (Fig. 6d).

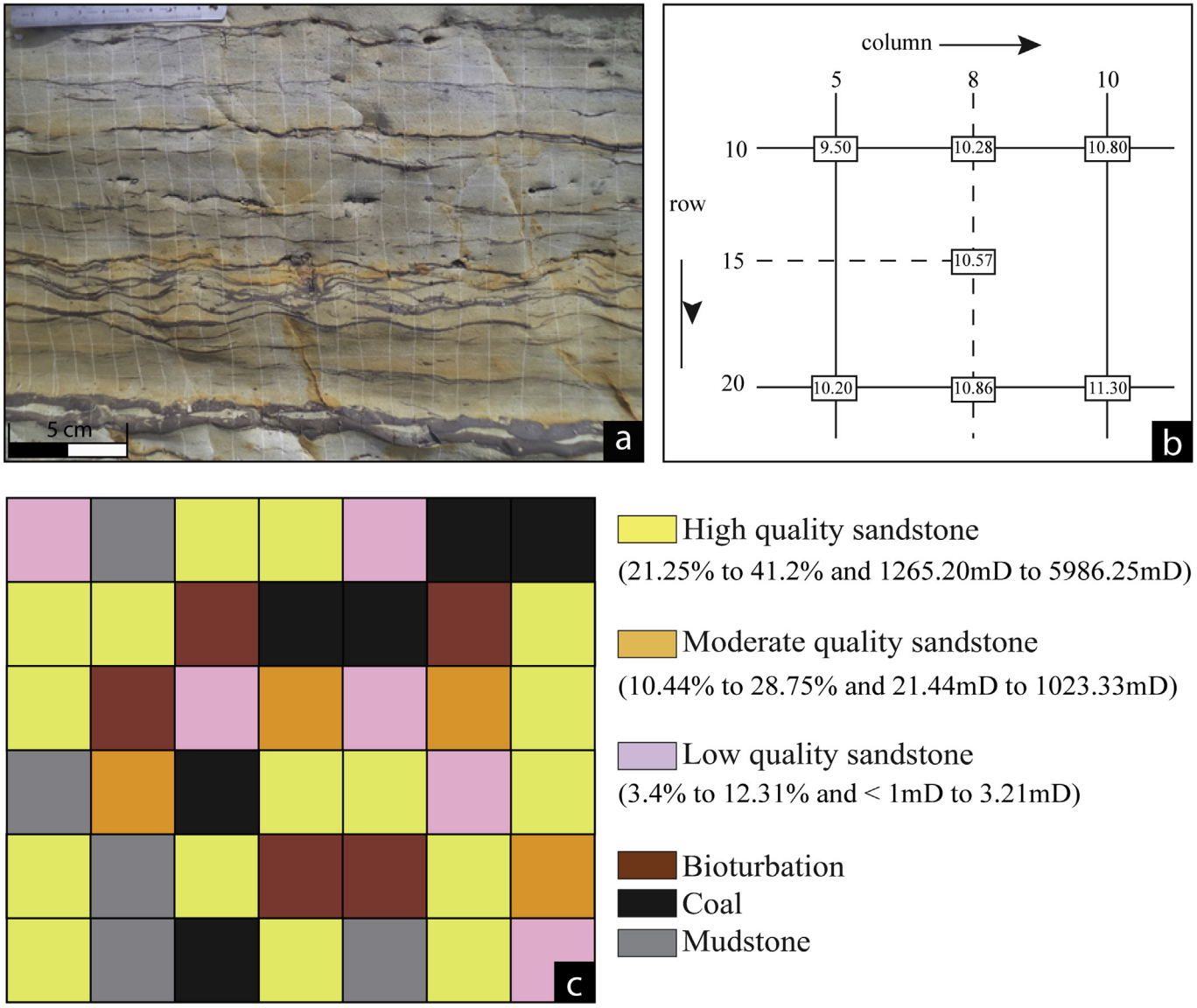

Figure 4. Gridding and modeling approach. (a) example of outcrop facies grid marking for permeability measurements for a facies flow modeling; (b) bilinear interpolation for grid population with permeability values in flow modeling; (c) distribution of sandstone quality with three different porosity and permeability ranges depending on the quality of sandstone.

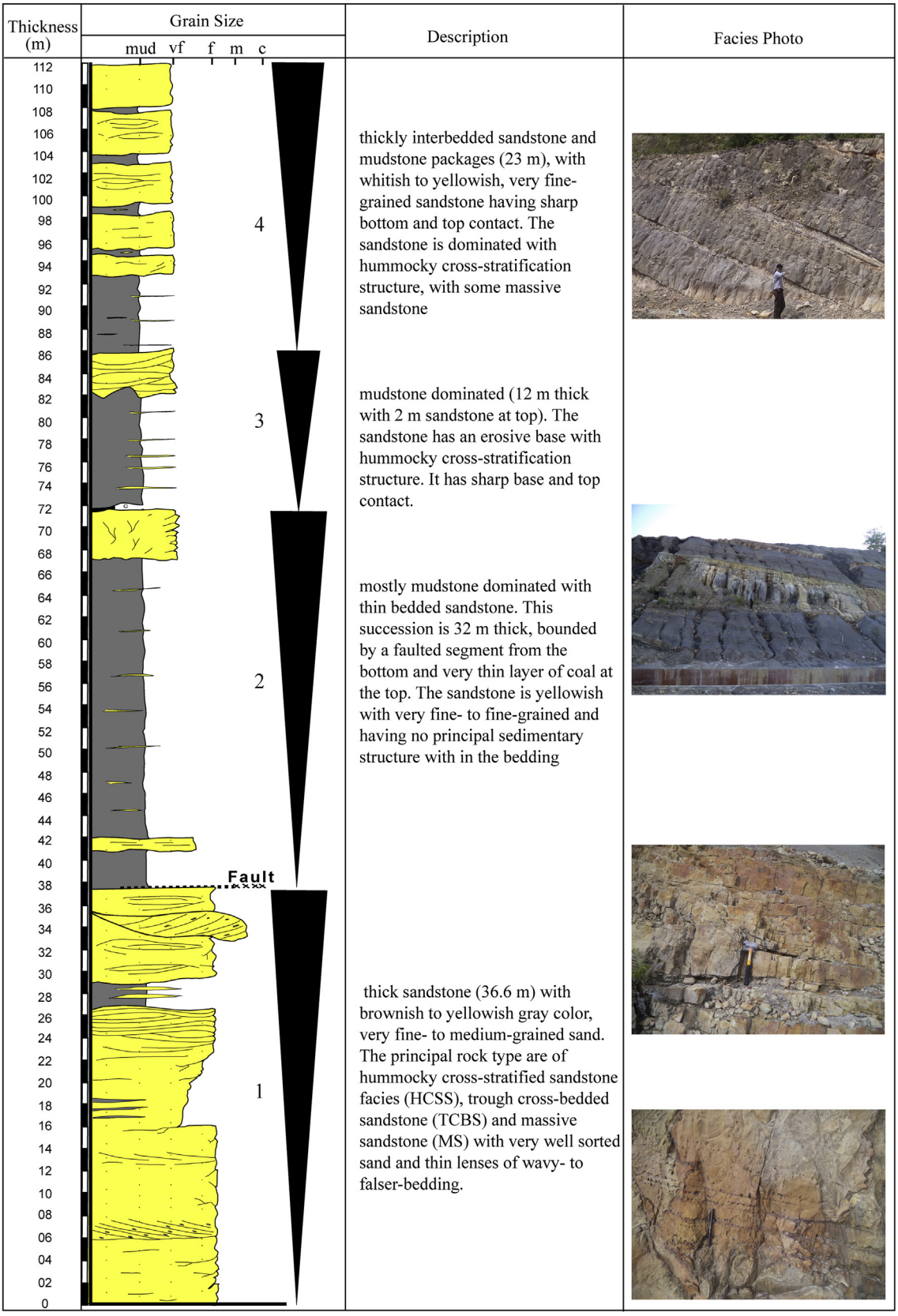

Figure 5. Sedimentary log showing sedimentology, facies and stratigraphic surfaces and units with description, Sandakan Formation. It represents a total of 112 m thick succession with four units. Each unit comprises different facies which are defined by combination of sedimentary structures.

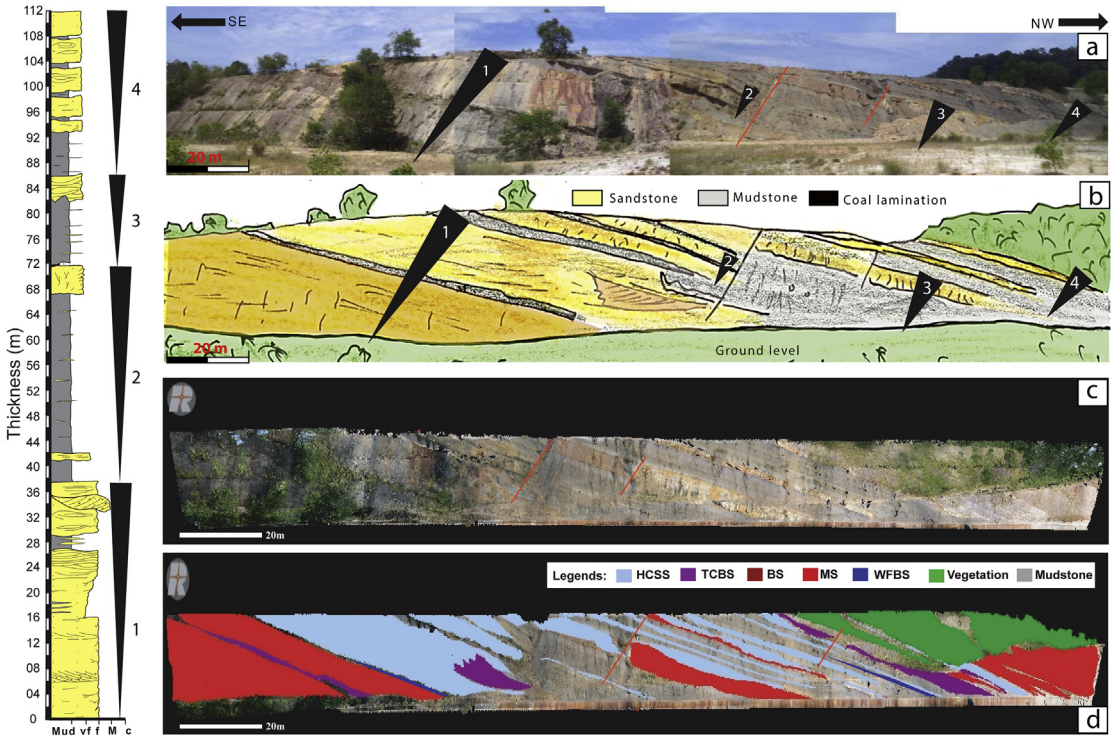

Figure 6. The hierarchy of four coarsening upward units (stratigraphic log at left) with outcrops; (a) and (b) outcrop photograph and sketch representing the units and lithology (sandstone, mudstone and some coal lamination) distribution with two normal faults marked between units 2 and 3; (c) LiDAR point cloud with texturing of high resolution photograph represent the full section, the mudstones show thickness of <1 m thick and sandy facies, which thicken upward, vary from 10 m thick at base and thin up to 4 m towards the top of the unit; (d) detailed description of each of the sandstone facies static connectivity with different colors representing the thicknesses with its lateral and vertical extents.

The segmented facies distribution mapped to produce a digital outcrop model (DOM) derived from field observations and high-resolution LiDAR which shows the distribution of sandstone facies type and mudstone with distinct boundaries (Fig. 6d). This distinctness allows comparing different structures at field scale observation and triangulation of point-clouds of different types of sandstone facies with different color codes. This trait has also allowed precise measurements of dimensions in different sandstone bodies (width and thicknesses) as well as vertical stacking patterns with different lithologies.

This approach of qualitative characterization enabled detailed description of individual facies, facies relationship, and the geometries marked on the main outcrop in the field. Transformation of the LiDAR data into DOM, which provides (1) architectural style and distribution of sandstone facies in the outcrop (both vertical and spatial), (2) quantification of shape and dimension of different sandstone facies, and (3) information on the static connectivity between sand-dominated geobodies (HCSS, TCBS and MS are interpreted as reservoir facies whereas BS and WFBS is classified as a non-reservoir facies).

4.3. Sandstone facies connectivity

Prior to the generation of the facies/outcrop connectivity and flow models, outcrop log data were utilized as inputs to the modeling software. The outcrop log data is crucially used to: (1) verify the geocellular model against key surface interpretation in the logs; (2) utilize the sedimentological information as conditioning data for facies modeling; and (3) quality control of final facies flow simulation.

At outcrop scale, the 112 m thick Sandakan Formation represents thick successions of sandstone and siltstone bounded by flooding surfaces with coarsening upward trends. Sandstone continuity is good (tens of meters) vertically as well as laterally up to hundreds of meters (Fig. 6a and b), forming a typical outcrop analogue to petroleum pays encountered in producing wells (Weber, 1982; Hamilton, 1991; Brandsæter et al., 2005; Nyberg and Howell, 2016). Vertical continuous units of sandstone are compartmentalized by mudstone and poorly lithified siltstone which affects the connectivity and continuity. Analysis on LiDAR provided lateral and vertical profiling which helps in delineating gross architectural elements (Fig. 6d). LiDAR data showed the variability in sandstone facies connectivity accurately, and represented the true lithological features which are not accessible through traditional field studies. To assess whether the laterally persistent bioturbated and mudstone unit's act as either barrier or baffles to vertical and lateral connectivity, LiDAR model demonstrates the application of geobodies and facies static connectivity. This can permit the spatial accuracy and resolution to be enhanced at facies scale.

The HCSS facies is preserved throughout the outcrop with thick to thin bedded sandstone units. The TCBS, BS and WFBS are thin bedded characteristics with abundance of coal laminations. The MS is thick and clean with good lateral extent. The outcrop bedding shows the grain size variation from very fine- to fine-grained, moderately- to well-sorted (bi-model) and coarsening upward trends. Most of the thick bedded sandstone (2–10 m) shows good lateral continuity and connectivity (tens to hundreds of meters), whereas, the vertical discontinuity is introduced by flooding surfaces. Facies scale permeability varies from <1 to 6000 mD (Fig. 7;

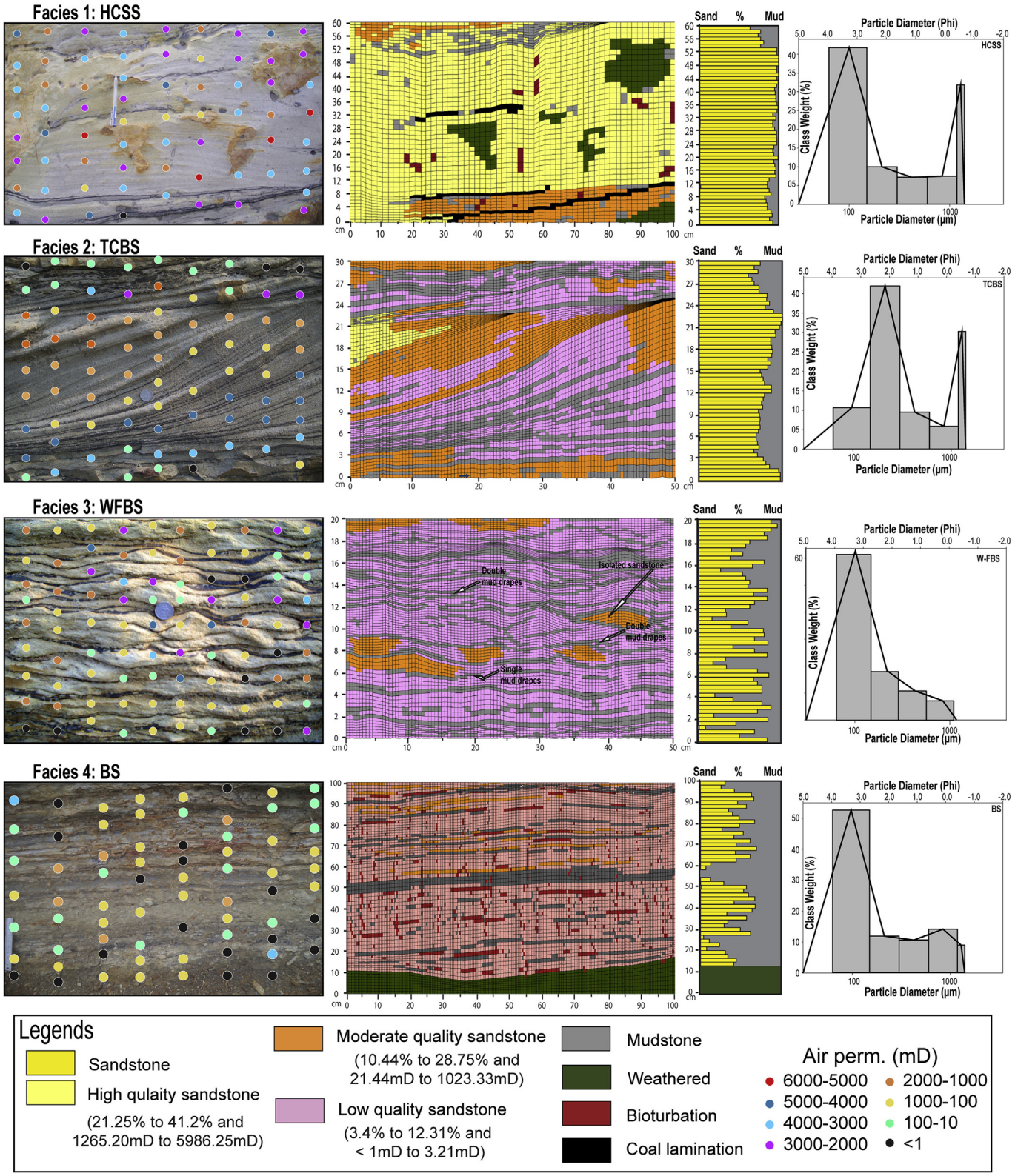

Figure 7. The variation in sandstone quality depending upon the types of and percentages of sandstone and mudstone. The distribution of percentages of sand and mud are representing in each sub-layers with horizontal histograms. Facies 1: HCSS – Hummocky cross-stratified sandstone represents the most laterally extensive and high quality sandstone reservoir; Facies 2: TCBS – the TCBS facies type showed dependence of connectivity on the lithology, architecture and angle of bedding; Facies 3: WFBS – low quality sandstone essentially due to the high percentage of mudstone and very fine-grained sandstone and Facies 4: BS – high bioturbation which represents low permeability especially at horizontal connectivity. The burrows filled with mud act as impermeable pathways in low quality sandstone.

Facies 1: HCSS). While the HCSS shows the highest permeability, all the facies types show a wide range of variability such that, the HCSS contains 2000–6000 mD, the TCBS 4000–1500 mD and BS and WFBS <500 mD, on average. As interpreted based on the facies and grain characteristics, the WFBS and BS act as permeability barriers, while the massive coarse grained sands contain highest permeability (Fig. 7; Facies 3: WFBS and Facies 4: BS).

The outcrop exposure used for the facies connectivity and flow modeling were ranging from 1–100 cm thick (Fig. 7). The measurements of permeability values were taken on each of the grid, which were bilinearly extrapolated to populate the surface with permeability variation. The porosity values obtained so were substituted for each layer of grids. The variations in sandstone quality were marked with high quality sandstone (HQS; porosity 21.25%–41.2% and permeability 1265.20–5986.25 mD), moderate quality sandstone (MQS; porosity 10.44%–28.75% and permeability 21.44–1023.33 mD) and low quality sandstone (LQS; porosity 3.4%–12.31% and permeability < 1 mD to 3.21 mD) depending upon the types and percentages of sandstone and mudstone (Fig. 7). Detailed analysis of the sedimentology and interpretation of four major sandstone facies was used as a framework to demonstrate the sandstone facies connectivity and flow dynamics.

4.3.1. Hummocky cross-stratified sandstone (HCSS)

Hummocky cross-stratified sandstone represents the most laterally extensive and high quality sandstone reservoir in Sandakan Formations in terms of porosity and permeability. The outcrop used for connectivity and flow model (100 cm × 60 cm) is clean sandstone with thin laminations of coal (Fig. 7, Facies 1: HCSS). The flow is distributed with high quality sandstone (HQS), moderate quality sandstone (MQS) and low quality sandstone (LQS) (Fig. 7). It has been observed that the top and bottom sandstone is interfingered with HQS and MQS, whereas, the middle section is of HQS. The weathered surface is marked by green and bioturbation in red. It has been observed that the percentage of sand in each sub layer grid block is >70% in all HCSS facies with bimodal distribution of grain size (−1.0ϕ to 4.0ϕ) (Fig. 7; Facies 1: HCSS). The grids were also marked with bioturbation and coal interlaminated sandstone which acts as a flow baffles.

4.3.2. Trough cross-bedded sandstone (TCBS)

Modeling the TCBS facies type showed dependence of connectivity on the lithology, architecture and angle of bedding (Fig. 7; Facies 2: TCBS). It has been observed that the percentage of sandstone and mudstone varies with in 20%–99% in this facies, which causes the heterogeneity in sandstone reservoir quality. This sandstone facies type is characterized by very fine- to fine-, moderately-sorted to well-sorted sand grains (bimodal) that form HQS to LQS. In these facies types, high permeable sandstones are distributed at the thicker edge of layers and sub-layers with minimal mud contents which gradually changes to MQS and finally to LQS toward the narrow edge (Fig. 7; Facies 2: TCBS). The top and bottom of TCBS facies layers act as strong baffles due to the occurrences of mudstone. In some case it has been observed that the quality of sandstone is mostly LQS due to the occurrence of thin mudstone lamina (<0.5 cm) which affects the flow path.

4.3.3. Wavy- to flaser-bedded sandstone (WFBS)

The outcrop exposure used for this facies is of discontinuous sandstone-mudstone packages, which reveals large variations in lateral continuity and vertical connectivity (Fig. 7). As could be expected, this facies depicts low quality sandstone (LQS; 3.4%–12.31% and <1 mD to 3.21 mD) essentially due to the high percentage of mudstone and very fine-grained nature (<3ϕ) (Fig. 7; Facies 3: WFBS). Two conditional scenarios are possible in this sandstone facies; either the drapes connect vertically forming double mud drapes with percentage of sand-mud randomly distribute i.e. 50% sand 50% mud or they can be continues as a single drape with some high value of permeability and porosity (Fig. 7; Facies 3: WFBS).

4.3.4. Bioturbated sandstone (BS)

The process of bioturbation displaces and mix sediment grains by burrowing, feeding activities of organisms. It has relocated sediments with bimodal distribution (−1.0ϕ to 4.0ϕ). The activity of organisms within the substrate adds sedimentary heterogeneity, and alters horizontal and vertical permeability. In the case of studied area, the bioturbation is either of high intensity or low intensity. Here we take the scenario of BS facies with high bioturbation which represents low permeability especially at horizontal connectivity (Fig. 7; Facies 4: BS). The outcrop used for analyzing permeability distribution and sandstone quality distribution is highly bioturbated sandstone. The burrows filled with mud act as impermeable pathways in low quality sandstone. As more than 60% of sub-layer in each layer is mudstone with very fine-grained sandstone, this lithological characteristic might be reason for the restriction in flow (Fig. 7; Facies 4: BS). In addition, the highly bioturbated nature, might have significantly reduced the reservoir quality, producing non-reservoir interval.

5. Discussion

5.1. Outcrop and facies flow models

Precise elucidation of outcrop scale facies heterogeneity depends on enhancement of accuracy by increasing the sample size (Narayanan et al., 1999). It reduces the standard error of the observed dataset (which is still a sub-sample of the entire stratigraphic volume) and, therefore, reduces the uncertainty in the static modeling (Enge et al., 2007). By using DOMs as initial data to extract the input parameters, uncertainties related to industry-standard geological modeling approaches can be reduced by filling-in the gaps in resolution between traditional data, such as seismic survey and well data (Brandsæter et al., 2005). Some of the conditioning parameters (i.e. geobody dimension, connectivity) that are difficult, if not impossible, to estimate from subsurface reservoirs can be extracted directly from the DOM. And these data may then be used as input for the stochastic modeling. The application of DOM approach improves the size of the outcrop data sample and, therefore, reduces uncertainty in the outcrop-derived data.

The facies association information in the studied outcrop logs was up-scaled according to the distribution of facies in digital outcrop data for zonation of sand bodies (Fig. 8A and B). Each zone was modeled independently. It corresponds to the high resolution outcrop sandstone facies architectural elements identified from the detailed outcrop characterization as presented by previous studies elsewhere (e.g. Fabuel Perez et al., 2009a,b, 2010; Graham et al., 2015; Howell et al., 2015; Sahoo and Gani, 2015; Newell and Shariatipour, 2016; Seers, 2017; Siddiqui et al., 2017a,b). Although, the final facies model shows similar facies distribution and outcrop architecture to that observed in the outcrop (Fig. 6) differences are identified in some areas of the model. The most important difference is associated with the lateral and vertical distribution of thin bodies which cannot be easily derived from stratigraphic logs. To reflect and accurately define shape and dimensions of input parameters, a

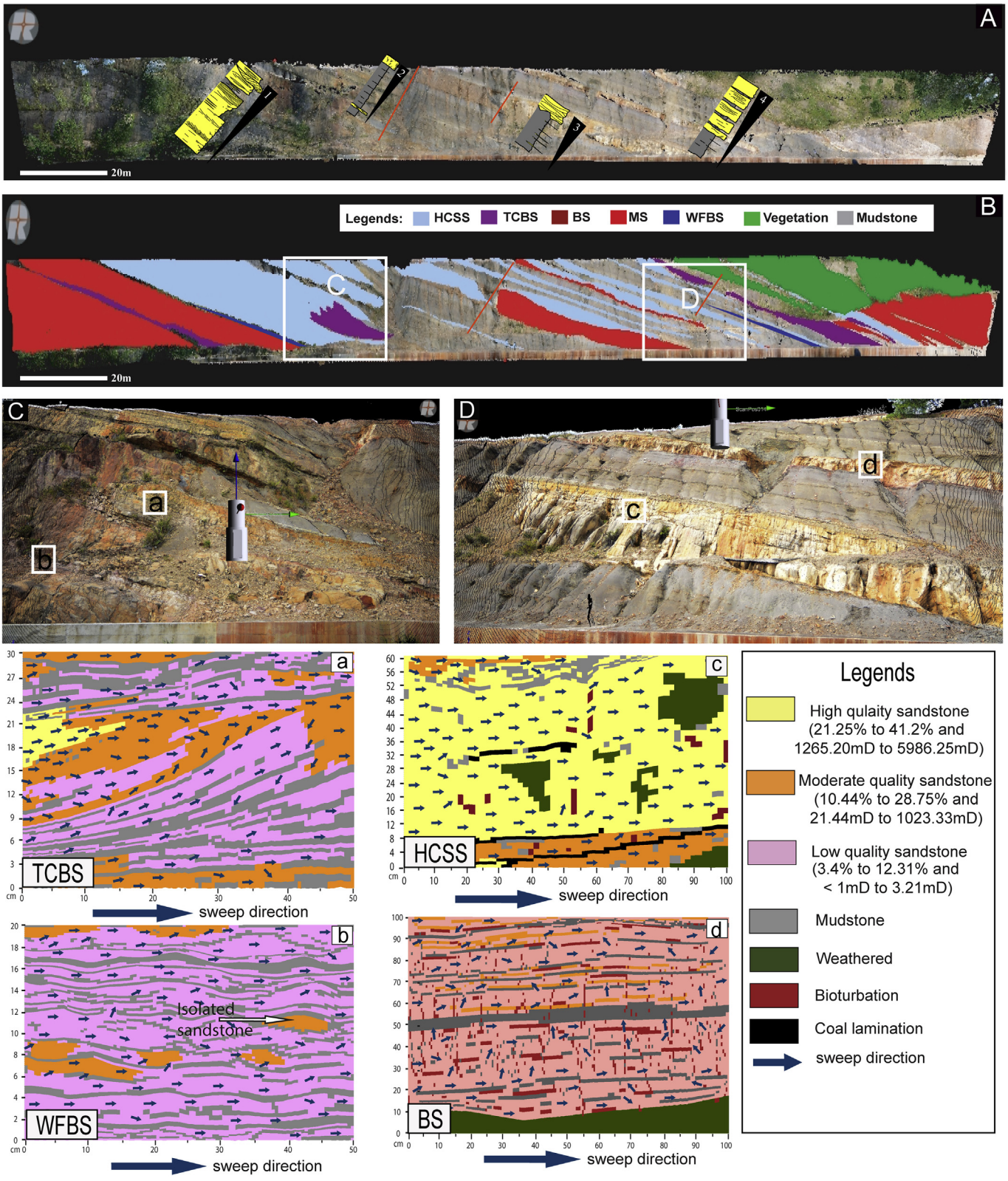

Figure 8. (A) Log data is up scaled according to the distribution of facies in digital outcrop (LiDAR) data for zonation of sand bodies; (B) object based technique is further improvise at each of the different set of facies to create sandstone facies object and bodies with its connectivity and vertical/lateral; (C) and (D) a discrete parameter is defined in the static model that can better visualized the 2D spatial connectivity of net-reservoir facies in final model; (a) TCBS facies show distortion of thin but laterally extensive shale (mudstone), especially troubling; (b) WFBS show the vertical flow performance is almost zero or < 0.1 mD due to the discontinuity in layer caking, whereas, the horizontal sweep is linear to the bedding surface, which only affected by double mud drapes or bioturbation; (c) HCSS shows flow tortuosity or sweep is uniform with less dispersion in HQS; and (d) other type of non-net-reservoir sandstone (BS) shows fluid flow becomes increasingly anisotropic due to greater amounts of burrow interpenetrations across layers and grid block.

facies model by using LiDAR technique was constructed (Fig. 8B). This object based technique is further improvised at each of the different set of facies to create sandstone facies object and bodies (with appropriate characteristic and flow heterogeneities) that represent elements observed as in the depositional model (Tyler et al., 1994; Pringle et al., 2006; Fabuel-Perez et al., 2009a,b; Daidu et al., 2013). It is essential for simplification and independent validation of the reservoir heterogeneity of different sandstone facies. The sand rich facies (HCSS, TCBS and MS) are classified as net-reservoir facies and BS, WFBS and mudstone are classified as non-net-reservoir facies. Based on the net and non-net reservoir classification, a discrete parameter was then defined in the static model that more accurately visualized the 2D spatial connectivity of net-reservoir facies in final model (Fig. 8C and D).

The HCSS facies represents the most laterally extensive facies in the studied outcrops and thus accurate identification of its lateral geometry and continuity was made through digitization in DOM (Fig. 8B). Other facies types, namely, BS, MS, WFBS and TCBS were also modeled with high resolution and photographic analysis with well-marked boundaries. By simulating the flow in four main sandstone bodies, HCSS type of sandstone at centimeter scale (in this case water) shows uniform flow or sweep with less dispersion in HQS (21.25%–41.2% and 1265.20–5986.25 mD) and MQS (10.44%–28.75% and 21.44–1023.33 mD), due to good quality of sandstone in terms of permeability variation laterally and vertically. The rock heterogeneities in terms of mud and coal lamination affect the flow path patterns which allow movement of fluid through down-dip or up-dip sub-layers (Fig. 8c). Overall, in case of HCSS the flow is uniform and linear, followed by sub-layer gridding. While performing the flow simulation, TCBS facies showed distortion by thin laterally extensive mudstone and found to be LQS (3.4%–12.31% and <1 mD to 3.21 mD) where the mudstone occurred and the control exercised by mudstone layers is explicit in the modeled fluid flow (Fig. 8a). Three scenarios of flow path were identified: (1) connected path, which allowed the flow to move along the bedding and sub-layers vertically and horizontally (Snedden et al., 2007); (2) isolated path, which follow only to those connected sub-layers which are isolated in the whole area and (3) dead end path, which are not sweeps (Kjønsvik et al., 1994) (Fig. 8a). These scenarios reveal that the heterogeneity can occur within the thick sandstone facies.

It was observed that the vertical flow performance of WFBS was almost zero or <0.1 mD due to the discontinuity in sandstone layers (Fig. 8b). The horizontal sweep was linear/parallel to the bedding surface, which only affected by double mud drapes or bioturbation. This heterogeneity can be visualized by the occurrences of individual sandstone and mudstone layers in exposed section (Fig. 7). The other type of non-net-reservoir sandstone (BS) showed fluid flow to be increasingly anisotropic due to greater amounts of burrow interpenetrations across layers and grid blocks (Fig. 8d). As such, low volumes of bioturbation result in only minor influences on fluid flow. At higher volumes of bioturbation, greater burrow interconnectivity occurs and results in a deterioration or enhancement of vertical and horizontal permeability due mud or sand fill in borrows (Fig. 8d). Therefore, in more heterolithic sandstone, like BS, lateral and vertical variations in permeability show spatially non-correlated patterns.

5.2. Evaluation of uncertainties

Based on the experiments and the results presented in the previous section we have conducted and developed a workflow to improve the accuracy of the outcrop digital data for high resolution flow simulation. The method helps to reduce the degree of uncertainty associated with the outcrop accessibility and data size (Fabuel-Perez et al., 2010). By improvising the outcrop with DOM's through LiDAR data, we have demonstrated a tool for defining the facies zonation accurately and geocellular flow model for different sets of sandstone facies.

Although the work improves and reflects accurately of the observed outcrop geology, there remains some uncertainty that need to be considered while performing such workflow. The uncertainties that may arise during the analysis can be grouped as:

(1) Uncertainties related to lateral extent of facies distribution and its accurate estimation. Although vertical distribution provides a good control of facies distribution, but its estimation of lateral continuity is tenuous and is often riddled with errors (Matthews et al., 2008; Fabuel-Perez et al., 2009a; Newell and Shariatipour, 2016), essentially due to the inherent characteristics of facies, that gradually grade to other facies types. To highlight this issue, we plotted different sets of sandstone facies with high resolution digital point cloud data through LiDAR data acquisition (Fig. 8B) to ensure close affinity between the field observation data modeled data.
(2) Uncertainties related to errors in processing of DOMs. They include errors caused during alignment of GPS scan positions, triangulation of facies distribution and inaccurate registration and texturing of outcrop point clouds and photographs (Buckley et al., 2008). These types of errors and uncertainties can be minimized by comparing with ground field observation, LiDAR model and static connectivity.
(3) Uncertainties related to 3D morphology in the point clouds interpretation. Stratigraphic surfaces show only 2D facies distribution with no 3D geometry, introducing error in flow simulation. Consequently interpolation of permeability and distribution of three types of sandstone quality (HQS, MQS and LQS) inherit uncertainties in their permeability distribution. These uncertainties are considerably reduced by using high resolution geocellular grid distribution in each of the four sandstone facies (Fig. 8). It shows that resultant flow models are mostly pragmatic due to the interconnected sandstone rather than the quality of sandstone.

6. Conclusions

We demonstrated a workflow to build high resolution geocellular sandstone facies architecture and digital outcrop fluid flow model. This experimental approach has implication on flow simulation at high resolution outcrop scale for analogue studies of reservoir simulation models. Combination of digital outcrop point-clouds and images provides a detailed spatial template distribution of sandstones to model key surfaces for an accurate outcrop connectivity model.

The workflow follows methods to populate the point with different sandstone type resulting in a 2D facies model with high precision. The model shows vertical and horizontal connectivity with heterogeneities observed in the outcrop through a 2D static connectivity model which can be analogue to sub-surface modeling. The facies of HCSS type sandstones represents the most laterally extensive facies and accurate identification of lateral dimension was made and digitized in DOM. Whereas, the other facies of BS, MS, WFBS and TCBS were modeled with high resolution and photographic analysis with well-marked boundaries. The sand rich facies (HCSS, TCBS and MS) are classified as net-reservoir facies and BS, WFBS and mudstone are classified as non-net-reservoir facies. We also presented here a workflow to improve the accuracy of the outcrop digital data for high resolution flow simulation. This helps to diminish the degree of uncertainty

associated with the outcrop accessibility and data size. The combination of DOM with accurately positioned high resolution sedimentary outcrop logs allows quality control of flow model. Sandstone facies distribution (lateral and vertical continuity and geometry) and correction of the geocellular model, in an area showing errors related to the interpolation of the surfaces with permeability and quality of sandstone. These results can have wider implications on assessment, selection and application of outcrop based analogue models for subsurface reservoirs.

Acknowledgment

The authors would like to thank Institute of Hydrocarbon Recovery, Universiti Teknology PETRONAS and Petroliam Nasional Berhad, Malaysia Oil and Gas Company for funding this research project (YUTP cost # 0153AA-E79). We thank GPS Lands (M) Sdn. Bhd. Team for providing RIEGL RiScan Pro Instruments for LiDAR data acquisition and to facilitate with data acquisition and filtration. There is no conflict of interest including any financial, personal or other relationships with other people or organizations.

References

Aigner, T., Asprion, U., Hornung, J., Junghans, W.D., Kostrewa, R., 1996. Integrated outcrop analogue studies for Triassic alluvial reservoirs: examples from southern Germany. Journal of Petroleum Geology 19, 393–406.

Alexander, J., 1993. A discussion on the use of analogues for reservoir geology. Geological Society of London, Special Publications 69, 175–194.

Bell, R., Jessop, R., 1974. Exploration and geology of the West Sulu basin, Philippines. The APEA Journal 14, 21–28.

Bellian, J.A., Kerans, C., Jennette, D.C., 2005. Digital outcrop models: applications of terrestrial scanning lidar technology in stratigraphic modeling. Journal of Sedimentary Research 75, 166–176.

Brandsæter, I., McIlroy, D., Lia, O., Ringrose, P., Næss, A., 2005. Reservoir modelling and simulation of Lajas Formation outcrops (Argentina) to constrain tidal reservoirs of the Halten Terrace (Norway). Petroleum Geoscience 11, 37–46.

Buckley, S.J., Howell, J., Enge, H., Kurz, T., 2008. Terrestrial laser scanning in geology: data acquisition, processing and accuracy considerations. Journal of the Geological Society 165, 625–638.

Buckley, S.J., Kurz, T.H., Howell, J.A., Schneider, D., 2013. Terrestrial lidar and hyperspectral data fusion products for geological outcrop analysis. Computers & Geosciences 54, 249–258.

Caers, J., Zhang, T., 2004. Multiple-point Geostatistics: a Quantitative Vehicle for Integrating Geologic Analogs into Multiple Reservoir Models, pp. 383–394.

Caers, J.K., Srinivasan, S., Journel, A.G., 2000. Geostatistical quantification of geological information for a fluvial-type North Sea reservoir. SPE Reservoir Evaluation and Engineering 3, 457–467.

Chung, K.W., Sum, C.W., Rahman, A.H., 2015. Stratigraphic succession and depositional framework of the Sandakan formation, Sabah. Sains Malaysiana 44 (7), 931–940.

Clemetsen, R., Hurst, A., Knarud, R., Omre, H., 1990. A computer program for evaluation of fluvial reservoirs. In: North Sea Oil and Gas Reservoirs—II. Springer, pp. 373–385.

Comexco, Inc, 1993. Hydrocarbon potential of the Sibutu block (GSEC-70). The philodrill coporation, report No. Bdi. Philodrill 5, 1–93.

Daidu, F., Yuan, W., Min, L., 2013. Classifications, sedimentary features and facies associations of tidal flats. Journal of Palaeogeography 2, 66–80.

Egeland, T., Georgsen, F., Knarud, R., Omre, H., 1993. Multifacies modelling of fluvial reservoirs. In: Presented at 68th Annual Technical Conference and Exhibition of the Society of Petroleum Engineers Held in Houston, Texas. https://doi.org/10.2118/26502-MS.

Enge, H.D., Buckley, S.J., Rotevatn, A., Howell, J.A., 2007. From outcrop to reservoir simulation model: workflow and procedures. Geosphere 3, 469–490.

Fabuel-Perez, I., Hodgetts, D., Redfern, J., 2009a. A new approach for outcrop characterization and geostatistical analysis of a low-sinuosity fluvial-dominated succession using digital outcrop models: upper Triassic Oukaimeden Sandstone Formation, central High Atlas, Morocco. AAPG Bulletin 93, 795–827.

Fabuel-Perez, I., Redfern, J., Hodgetts, D., 2009b. Sedimentology of an intra-montane rift-controlled fluvial dominated succession: the upper Triassic Oukaimeden sandstone formation, central high Atlas, Morocco. Sedimentary Geology 218, 103–140.

Fabuel-Perez, I., Hodgetts, D., Redfern, J., 2010. Integration of digital outcrop models (DOMs) and high resolution sedimentology–workflow and implications for geological modelling: Oukaimeden Sandstone Formation, High Atlas (Morocco). Petroleum Geoscience 16, 133–154.

Falivene, O., Arbus, P., Gardiner, A., Pickup, G., Muoz, J.A., Cabrera, L., 2006. Best practice stochastic facies modeling from a channel-fill turbidite sandstone analog (the Quarry outcrop, Eocene Ainsa basin, northeast Spain). AAPG Bulletin 90, 1003–1029.

Franke, D., Savva, D., Pubellier, M., Steuer, S., Mouly, B., Auxietre, J.-L., Meresse, F., Chamot-Rooke, N., 2014. The final rifting evolution in the South China Sea. Marine and Petroleum Geology 58, 704–720.

Futalan, K., Mitchell, A., Amos, K., Backe, G., 2012. Seismic facies analysis and structural interpretation of the Sandakan Sub-Basin, Sulu Sea, Philippines. AAPG Search and Discovery Article 30254.

Graham, G.H., Jackson, M.D., Hampson, G.J., 2015. Three-dimensional modeling of clinoforms in shallow-marine reservoirs: Part 2. Impact on fluid flow and hydrocarbon recovery in fluvial-dominated deltaic reservoirs. AAPG Bulletin 99 (6), 1049–1080.

Graves, J.E., Swauger, D.A., 1997. Petroleum Systems of the Sandakan Basin, Philippines, pp. 799–813.

Hall, R., 1996. Reconstructing cenozoic SE Asia. Geological Society, London, Special Publications 106, 153–184.

Hall, R., 2002. Cenozoic geological and plate tectonic evolution of SE Asia and the SW Pacific: computer-based reconstructions, model and animations. Journal of Asian Earth Sciences 20, 353–431.

Hall, R., 2013. Contraction and extension in northern Borneo driven by subduction rollback. Journal of Asian Earth Sciences 76, 399–411.

Hall, R., Morley, C.K., 2004. Sundaland basins. In: Continent-Ocean Interactions Within East Asian Marginal Seas. AGU, Washington DC, pp. 55–85.

Hamilton, W.B., 1979. Tectonics of the Indonesian Region. US Govt. Print. Off, pp. 34–88.

Hamilton, D., 1991. Reservoir heterogeneity at seventy-six west field Texas: an opportunity for increased Oil recovery from barrier/Strandplain reservoirs of the Jackson-Yegua trend by geologically targeted infill drilling. In: Paper Presented at the SPE Annual Technical Conference and Exhibition. https://doi.org/10.2118/22672-MS.

Higgs, K.E., Arnot, M.J., Browne, G.H., Kennedy, E.M., 2010. Reservoir potential of Late Cretaceous terrestrial to shallow marine sandstones, Taranaki Basin, New Zealand. Marine and Petroleum Geology 27, 1849–1871.

Hodgetts, D., 2013. Laser scanning and digital outcrop geology in the petroleum industry: a review. Marine and Petroleum Geology 46, 335–354.

Howell, J.A., Martinius, A.W., Good, T.R., 2015. The application of outcrop analogues in geological modelling: a review, present status and future outlook. Geological Society, London, Special Publications 387, 1–25.

Hurst, A., Verstralen, I., Cronin, B., Hartley, A., 1999. Sand-rich fairways in deep-water clastic reservoirs: genetic units, capturing uncertainty, and a new approach to reservoir modeling. AAPG Bulletin 83, 1096–1118.

Hutchison, C.S., 1989. Geological Evolution of South-east Asia. Clarendon Press; Oxford University Press, Oxford [Oxfordshire]; New York, pp. 50–88.

Hutchison, C.S., 2005. Geology of North-West Borneo: Sarawak. Elsevier, Brunei and Sabah, pp. 175–177. ISBN: 978-0-444-51998-6.

Kjønsvik, D., Doyle, J., Jacobson, T., Jones, A., 1994. The Effects of Sedimentary Heterogeneities on Production from a Shallow Marine Reservoir-What Really Matters? Society of Petroleum Engineers, Richardson, TX (United States). https://doi.org/10.2118/28445-MS.

Krum, G., Johnson, C., 1993. A 3-D modelling approach for providing a complex reservoir description for reservoir simulations. The Geologic Modelling of Hydrocarbon Reservoirs. https://doi.org/10.1002/9781444303957.ch16.

Kurz, T.H., Buckley, S.J., Howell, J.A., Schneider, D., 2011. Integration of panoramic hyperspectral imaging with terrestrial lidar data. The Photogrammetric Record 26, 212–228.

Lee, D.T.C., 1970. Sandakan Peninsula, Eastern Sabah, East Malaysia. US Government Printing Office, pp. 45–77.

Levell, B., 1987. The nature and significance of regional unconformities in the hydrocarbon-bearing Neogene sequences offshore West Sabah. Geological Society of Malaysia Bulletin 21, 55–90.

Liu, K., Boult, P., Painter, S., Paterson, L., 1996. Outcrop analog for sandy braided stream reservoirs: permeability patterns in the Triassic Hawkesbury Sandstone, Sydney Basin, Australia. AAPG Bulletin 80, 1850–1865.

MacDonald, A.C., Halland, E.K., 1993. Sedimentology and shale modeling of a sandstone-rich fluvial reservoir: upper Statfjord formation, Statfjord field, northern North Sea. AAPG Bulletin 77, 1016–1040.

Majid, M.F., Suhaili Rahman, A.H., Azfar, M., 2017. Facies distribution and petrophysical properties of shoreface-offshore transition environment in Sandakan formation, NE Sabah Basin." IOP conference series. Earth and Environmental Science 88 (1), 22–34.

Mathew, M.J., Menier, D., Siddiqui, N., Kumar, S.G., Authemayou, C., 2016. Active tectonic deformation along rejuvenated faults in tropical Borneo: inferences obtained from tectono-geomorphic evaluation. Geomorphology 267, 1–15.

Matthews, J.D., Carter, J.N., Stephen, K.D., Zimmerman, R.W., Skorstad, A., et al., 2008. Assessing the effect of geological uncertainty on recovery estimates in shallow-marine reservoirs: the application of reservoir engineering to the SAIGUP project. Petroleum Geoscience 14, 35–44.

Mazlan, M.M., Rahman, A.H., 2007. Penecontemporaneous deformation in the nyalau formation (Oligo-Miocene), central Sarawak. Geological Society of Malaysia, Bulletin 53, 67–73.

Miall, A.D., 2006. Reconstructing the architecture and sequence stratigraphy of the preserved fluvial record as a tool for reservoir development: a reality check. AAPG Bulletin 90, 989–1002.

Narayanan, K., White, C., Lake, L., Willis, B., 1999. Response surface methods for upscaling heterogeneous geologic models. In: Presented at SPE Symposium on Reservoir Simulation, vol. 2, pp. 30–57.

Natali, M., Lidal, E.M., Viola, I., Patel, D., 2013. Modeling terrains and subsurface geology. In: Proceedings of Euro Graphics, State of the Art Reports (STARs), pp. 155–173.
Newell, A.J., Shariatipour, S.M., 2016. Linking outcrop analogue with flow simulation to reduce uncertainty in sub-surface carbon capture and storage: an example from the Sherwood Sandstone Group of the Wessex Basin, UK. Geological Society, London, Special Publications 2–436.
Noad, J., Neil, H., 1996. The Sedimentology of Miocene Shallow Marine Clastics of the Sandakan Formation of Eastern Sabah. American Geological Conference, Kota Kinabalu Sabah, pp. 119–133.
Nyberg, B., Howell, J.A., 2016. Global distribution of modern shallow marine shorelines. Implications for exploration and reservoir analogue studies. Marine and Petroleum Geology 71, 83–104.
PETRONAS, 1999. The Petroleum Geology and Resources of Malaysia: Chapter 24, pp. 573–588.
Pringle, J., Howell, J.A., Hodgetts, D., Westerman, A., Hodgson, D., 2006. Virtual outcrop models of petroleum reservoir analogues: a review of the current state-of-the-art. First Break 24 (3), 33–42.
Pringle, J., Westerman, A., Clark, J., Drinkwater, N., Gardiner, A., 2004. 3D high-resolution digital models of outcrop analogue study sites to constrain reservoir model uncertainty: an example from Alport Castles, Derbyshire, UK. Petroleum Geoscience 10, 343–352.
Sahoo, H., Gani, N.D., 2015. Creating three-dimensional channel bodies in LiDAR-integrated outcrop characterization: a new approach for improved stratigraphic analysis. Geosphere 11 (3), 777–785.
Sapin, F., Pubellier, M., Lahfid, A., Janots, D., Aubourg, C., Ringenbach, J.C., 2011. Onshore record of the subduction of a crustal salient: example of the NW Borneo Wedge. Terra Nova 23, 232–240.
Seers, T., Hodgetts, D., Wang, Y., Fadlelmula, M., 2017. Direct computation of fracture network equivalent porous medium properties using digital outcrop models. In: 79th EAGE Conference and Exhibition in Proceedings. https://doi.org/10.3997/2214-4609.201700647.
Siddiqui, N., Rahman, A.H., Sum, C.W., Mathew, M.J., Menier, D., 2014. Facies characteristics and static reservoir connectivity of some siliciclastic tertiary outcrop successions in Bintulu and Miri, Sarawak, east Malaysia. AAPG Search and Discovery, 51035.
Siddiqui, N., Rahman, A.H., Sum, C.W., Mathew, M.J., Menier, D., Muhammad, H., 2015. Modeling of littoral sandstones reveal variance in reservoir flow patterns: an example from nyalau formation, east Malaysia. Research Journal of Applied Sciences, Engineering and Technology 11, 176–184.
Siddiqui, N., Rahman, A.H., Sum, C.W., Mathew, M.J., Menier, D., 2016. Onshore sandstone facies characteristics and reservoir quality of nyalau formation, Sarawak, east Malaysia: an analogue to subsurface reservoir quality evaluation. Arabian Journal for Science and Engineering 41 (1), 267–280.
Siddiqui, N., Rahman, A.H., Sum, C.W., Mathew, M.J., Hassaan, M., Menier, D., 2017a. Generic hierarchy of sandstone facies quality and static connectivity: an example from the middle-late Miocene Miri formation, Sarawak basin, Borneo. Arabian Journal of Geosciences 10 (11), 237.
Siddiqui, N.A., Rahman, A.H., Sum, C.W., Murtaza, M., 2017b. Sandstone Facies Reservoir Properties and 2D-connectivity of Siliciclastic Miri Formation, Borneo, ICIPEG 2016. Springer, pp. 581–595.
Sima, A.A., 2013. An Improved Workflow for Image-and Laser-based Virtual Geological Outcrop Modelling (Ph.D. thesis). Publisher: The University of Bergen.
Slatt, R.M., Stone, C.G., Weimer, P., 2000. Characterization of slope and basin facies tracts, Jackfork Group, Arkansas, with applications to deepwater (turbidite) reservoir management. Presented at Deep-water reservoirs of the world: in Proceedings of Deep-water reservoirs of the world. In: 20th Annual Bob F. Perkins Research Conference, Gulf Coast Section-SEPM, pp. 87–103.
Slatt, R.M., Weimer, P., 1999. Turbidite systems Part 2: subseismic-scale reservoir characteristics. The Leading Edge 18, 562–567.
Snedden, J.W., Vrolijk, P.J., Sumpter, L.T., Sweet, M.L., Barnes, K.R., et al., 2007. Reservoir connectivity: definitions, examples and strategies. In: Paper Presentation at the International Petroleum Technology Conference Dubai, U.A.E.
Stauffer, P., 1967. Studies in the crocker formation, Sabah. Geological survey of Malaysia. Borneo Region Bulletin 8, 1–13.
Tan, D.N., Lamy, J., 1990. Tectonic evolution of the NW Sabah continental margin since the late eocene. Bulletin of the Geological Society of Malaysia 27, 241–260.
Tjia, H., Komoo, I., Lim, P., Surat, T., 1990. The Maliau basin, Sabah: geology and tectonic setting. Bulletin of the Geological Society of Malaysia 27, 261–292.
Tongkul, F., 1991. Tectonic evolution of Sabah, Malaysia. Journal of Southeast Asian Earth Sciences 6, 395–405.
Tongkul, F., 1992. Tectonic control on the development of the Neogene basins in Sabah, east Malaysia. In: Presented at Proceedings Symposium on the Tectonic Framework and Energy Resources of the Western Margin of the Pacific Basin, pp. 95–103.
Tongkul, F., 1994. The geology of northern Sabah, Malaysia: its relationship to the opening of the South China Sea basin. Tectonophysics 235, 131–147.
Tyler, K., Henriquez, A., Svanes, T., 1994. Modeling heterogeneities in fluvial domains: a review of the influence on production profiles. In: Yaris, J.M., Chambers, R.L. (Eds.), Stochastic Modelling and Geostatistics: Principles, Methods and Case Studies. AAPG. Computer Applications in Geology, vol. 3, pp. 77–89.
Weber, K., 1982. Influence of common sedimentary structures on fluid flow in reservoir models. Journal of Petroleum Technology 34 (3), 665–672.
Whittle, A., Short, G., 1978. The petroleum geology of the tembungo field, east Malaysia. In: Presented at Offshore South East Asia Conference, South East Asian Petroleum Exploration Society, pp. 29–39.
Willis, B.J., White, C.D., 2000. Quantitative outcrop data for flow simulation. Journal of Sedimentary Research 70 (4), 788–802.
Wilson, C.E., Aydin, A., Karimi-Fard, M., Durlofsky, L.J., Sagy, A., Brodsky, E.E., Kreylos, O., Kellogg, L.H., 2011. From outcrop to flow simulation: constructing discrete fracture models from a LIDAR survey. AAPG Bulletin 95, 1883–1905.